


ISSN: 0095-8972 (Print) 1029-0389 (Online) Journal homepage: <http://www.tandfonline.com/loi/gcoo20>


## A new phenylimidorhenium(V) compound containing the 2-[(2-hydroxyethylimino)methyl]phenol Schiff-base ligand: experimental and theoretical aspects

Smita Majumder, Jnan Prakash Naskar, Arnab Bhattacharya, Rakesh Ganguly, Pinki Saha & Shubhamoy Chowdhury

To cite this article: Smita Majumder, Jnan Prakash Naskar, Arnab Bhattacharya, Rakesh Ganguly, Pinki Saha & Shubhamoy Chowdhury (2015) A new phenylimidorhenium(V) compound containing the 2-[(2-hydroxyethylimino)methyl]phenol Schiff-base ligand: experimental and theoretical aspects, *Journal of Coordination Chemistry*, 68:4, 599-615, DOI: 10.1080/00958972.2014.996145


To link to this article: <http://dx.doi.org/10.1080/00958972.2014.996145>

 View supplementary material 

 Accepted author version posted online: 08 Dec 2014.  
Published online: 07 Jan 2015.

 Submit your article to this journal 

 Article views: 90

 View related articles 

 View Crossmark data 

 Citing articles: 2 View citing articles 

## A new phenylimidorhenium(V) compound containing the 2-[(2-hydroxyethylimino)methyl]phenol Schiff-base ligand: experimental and theoretical aspects

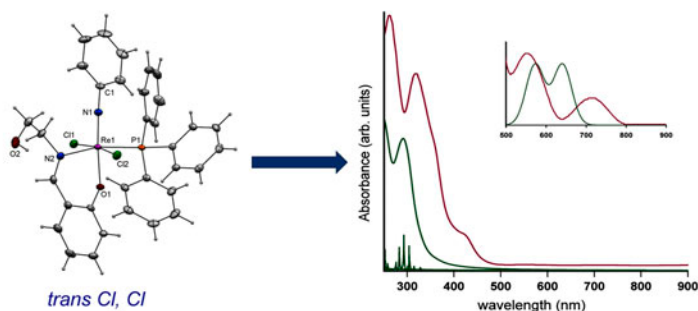
SMITA MAJUMDER<sup>†</sup>, JNAN PRAKASH NASKAR<sup>‡</sup>, ARNAB BHATTACHARYA<sup>†</sup>,  
RAKESH GANGULY<sup>§</sup>, PINKI SAHA<sup>†</sup> and SHUBHAMOY CHOWDHURY<sup>\*†</sup>

<sup>†</sup>Department of Chemistry, Tripura University, Tripura, India

<sup>‡</sup>Department of Chemistry, Inorganic Chemistry Section, Jadavpur University, Kolkata, India

<sup>§</sup>Division of Chemistry & Biological Chemistry, SPMS-CBC-01-18D, Nanyang Technological University, Singapore, Singapore

(Received 22 July 2014; accepted 10 November 2014)



Reaction of equimolar *trans*-[Re(NPh)(PPh<sub>3</sub>)<sub>2</sub>Cl<sub>3</sub>] with H<sub>2</sub>L, a 1 : 1 Schiff-base condensate of salicylaldehyde and ethanolamine, in chloroform gives *trans*-[Re(NPh)(HL)(PPh<sub>3</sub>)Cl<sub>2</sub>] (**1a**) in good yield. **1a** has been characterized by C, H, and N microanalyses, FTIR and UV-vis spectra. The X-ray crystal structure of **1a** reveals that it is an octahedral *trans*-Cl,Cl phenylimidorhenium(V) complex. The rhenium center has an 'N<sub>2</sub>OCl<sub>2</sub>P' coordination sphere. **1a** crystallizes in the monoclinic space group P2<sub>1</sub>/c with *a* = 11.2391(5), *b* = 16.4848(7), *c* = 16.3761(8) Å, *V* = 3034.0(2) Å<sup>3</sup> and *Z* = 4. The electrochemical aspects of **1a** have been studied. Electrochemical studies of **1a** in dichloromethane show a quasi-reversible Re(V) to Re(VI) oxidation at 1.128 V versus Ag/AgCl. This redox potential reasonably matches the calculated redox potential, 1.186 V versus Ag/AgCl. Geometry optimization of the *trans*-Cl,Cl **1a** vis-à-vis its *cis* analog, *cis*-Cl,Cl **1b**, have been performed at the level of density functional theory (DFT). It is revealed that **1a** is more stable than **1b** by 21.6 kcal per mole of energy in the gas phase.

**Keywords:** Phenylimidorhenium(V) complex; Schiff-base ligand; Electrochemistry; DFT and TDDFT calculations

\*Corresponding author. Email: [s.chowdhury@tripurauniv.in](mailto:s.chowdhury@tripurauniv.in)

## 1. Introduction

The chemistry of rhenium complexes has been the focus of renewed attention from applications. Rhenium complexes have been investigated energetically since the radionuclides of rhenium are optimal for therapeutic applications owing to its high  $\beta$ -ray energy and short half-life ( $^{186}\text{Re}$ :  $\beta_{\text{max}} = 1.070$  MeV,  $t_{1/2} = 90$  h;  $^{188}\text{Re}$ :  $\beta_{\text{max}} = 2.120$  MeV,  $t_{1/2} = 17$  h). They can target malignant tissues and have fairly fast clearance from the blood and other non-target tissues [1, 2].  $^{99\text{m}}\text{Tc}$ , the most widely used radionuclide for diagnostic imaging in nuclear medicine, is a group VII congener of rhenium. Thus, the chemistry of rhenium is almost akin to that of technetium. Therefore, the coordination chemistry of rhenium often supplements technetium, the mainstay in the field of radiopharmaceutical applications. In particular, the oxorhenium(V) and phenylimido rhenium(V) compounds are investigated for the design of novel radiopharmaceuticals. This is due to the fact that oxorhenium(V) compounds can readily be obtained from the reduction of perrhenate(VII) and can subsequently be stabilized by coordinating with a variety of ligands [3–8].

The chemistry of rhenium encompasses several formal oxidation states ranging from –I to VII. Oxidation of Re(V) complexes to Re(VII) is a pre-requisite in the catalytic cycle of an oxygen atom transfer (OAT) reaction [9]. The catalytic aspects of mono- and dinuclear methyloxorhenium(V) complexes as potential candidates for OAT reactions have been explored [10–12]. The catalytic propensities of *p*-tolylimidorhenium(V) complexes anchored with the picolinate ancillary ligand were studied in terms of the synthesis of *N*-substituted ethyl glycine esters from ethyl diazoacetate and amines [13]. Thus, there is interest in understanding the structures, spectroscopic properties, and redox behaviors of Re(V) complexes. This aspect of rhenium chemistry has kindled our interest to develop the chemistry of rhenium in this +V oxidation state.

2-[(2-Hydroxyethylimino)methyl]phenol ( $\text{H}_2\text{L}$ ), a Schiff-base ligand, seems to be a promising candidate in this perspective.  $\text{H}_2\text{L}$  can adopt different modes in its binding to metal centers – chelating as well as bridging, either in tridentate monoanionic ( $\text{HL}^{1-}$ ) form or in tridentate dianionic ( $\text{L}^{2-}$ ) form. Earlier, both  $\text{HL}^{1-}$  and  $\text{L}^{2-}$  have been employed to stabilize metal ions like Cu(II), Ni(II), Fe(III), Mn(II), Mn(III), and Zn(II) [14–22]. Thus, the coordination chemistry of the first row transition metal ions with  $\text{H}_2\text{L}$  is vast. Consequently, the nuclearities and geometries of the synthesized complexes are also diverse. Tetranuclear Cu(II), Ni(II), and Fe(II) with cubane structures are among these [20, 21]. Currently, we have been working to coordinate  $\text{H}_2\text{L}$  to rhenium [22].

Oxorhenium(V) complexes have been investigated for electronic structures and bonding situations using density functional theory (DFT) [23]. A large number of systems containing the oxorhenium(V) core have been studied by Gancheff et al. [24, 25]. Other systems like *p*-tolylimidorhenium(V) and tricarbonylrhenium(I) cores have also been studied by Machura et al. [13, 26, 27]. Time-dependent DFT (TDDFT) studies have been part of the investigations for explaining the electronic structures of oxorhenium(V) species to predict the reaction pathways primarily leading to catalytic aspects of oxorhenium(V) complexes [28].

Herein, we report the synthesis, characterization, structural elucidation, and redox behavior of a phenylimidorhenium(V) complex of  $\text{H}_2\text{L}$ . To gain further insights into the electronic structure, electronic transitions and redox behavior – calculations at the level of DFT and time-dependent density functional theory (TDDFT) were undertaken.

## 2. Experimental

### 2.1. Materials and physical measurements

Ammonium perrhenate (Sigma–Aldrich Chemicals) was used as received. *trans*-[Re(NPh)(PPh<sub>3</sub>)<sub>2</sub>Cl<sub>3</sub>] was prepared following a reported method [29] and using toluene in lieu of benzene as a solvent. Ethanolamine and salicylaldehyde were purchased from Sigma–Aldrich and were used without further purification. Microanalyses were performed with a Perkin-Elmer 2400II elemental analyzer. FTIR spectra were recorded as KBr pellets with a Perkin-Elmer FTIR-100 spectrophotometer. UV–vis absorption spectra of **1a** were recorded on a Perkin-Elmer Lambda 25 spectrophotometer and NMR spectra (in CDCl<sub>3</sub>) with a Bruker DPX300 spectrometer. Electrochemical experiments were performed on a BAS Epsilon electrochemical workstation (Model CV-50) under nitrogen in dry and degassed dichloromethane at 293 K. The supporting electrolyte was tetra-*n*-butylammonium perchlorate (TBAP) (0.1 M). The conventional three-electrode assembly was comprised of a glassy carbon (GC) working electrode, a platinum wire counter electrode and a Ag/AgCl reference electrode. All potentials reported herein are referenced to Ag/AgCl.

### 2.2. Synthesis of [Re(NPh)(HL)(PPh<sub>3</sub>)Cl<sub>2</sub>] (**1a**)

To a suspension of *trans*-[Re(NPh)(PPh<sub>3</sub>)<sub>2</sub>Cl<sub>3</sub>] (0.227 g, 0.25 mM) in toluene (10 mL) was added H<sub>2</sub>L (0.041 g, 0.25 mM) dissolved in 10 mL of toluene dropwise with stirring. The resulting reaction mixture was heated under reflux for 5 h. During reflux, the color changes from green to greenish brown. The resulting solution was evaporated under reduced pressure to dryness to have a gummy mass. The gummy mass was thoroughly washed with diethyl ether to get a dirty green powder. Yield: 145 mg, 75%; Anal. Calcd for C<sub>33</sub>H<sub>30</sub>N<sub>2</sub>O<sub>2</sub>Cl<sub>2</sub>PRE: C, 51.16; H, 3.90; N, 3.62. Found: C, 49.98; H, 3.82; N, 3.73%. FTIR (KBr, cm<sup>-1</sup>): (C=N) 1603 (*versus*); (Re≡N) 1025 (s). <sup>1</sup>H NMR (CDCl<sub>3</sub>, 300 MHz) ( $\delta$ , ppm): 4.01 (br. s, 2H); 4.09 (d, 2H, 5.1 Hz); 6.31 (d, 1H, 8.4 Hz); 6.90 (t, 1H, 7.2 Hz); 7.16 (t, 3H, 5.4 Hz); 7.32–7.35 (*m*, 11H); 7.53 (t, 2H, 6.3 Hz); 7.73–7.79 (*m*, 5H); 8.07 (d, 1H, 10 Hz); 8.38 (s, 1H). UV–vis (CH<sub>2</sub>Cl<sub>2</sub>),  $\lambda_{\max}$  ( $\epsilon$ , M<sup>-1</sup> cm<sup>-1</sup>): 263 (25,400); 319 (19,525); 360sh (12,295); 423sh (3260); 555 (118); 714 (84).  $\Lambda_M$  (acetonitrile): 0.20  $\Omega^{-1}$  cm<sup>2</sup> mol<sup>-1</sup> (non-electrolyte).

### 2.3. X-ray crystal structure determination

Single crystals of **1a**, suitable for X-ray structure determination, were selected by examination under a microscope. The appropriate single crystal of **1a** was mounted on a Bruker SMART APEX II CCD area detector diffractometer at 103 K using graphite monochromated Mo-K $\alpha$  radiation ( $\lambda = 0.71073$  Å). Intensity data of **1a** was reduced using SAINT [30] and the empirical absorption corrections were performed with SADABS [31]. The structure of **1a** was solved by direct methods and refined by full-matrix least-square methods based on  $|F|^2$  using SHELXL-97 [32]. All non-hydrogen atoms were refined anisotropically. Hydrogens were placed in calculated positions and constrained to ride on their parent atoms. All the calculations were carried out using SHELXS-97, SHELXL-97, and SHELXTL [32] programs. The crystallographic data for **1a** are summarized in table 1.

Table 1. Crystal data and structure refinement for **1a**.

Parameter	Complex <b>1a</b>
Formula	C <sub>33</sub> H <sub>30</sub> Cl <sub>2</sub> N <sub>2</sub> O <sub>2</sub> PRe
Formula weight	774.67
Crystal system	Monoclinic
Space group	P2 <sub>1</sub> /c
Unit cell dimensions	
<i>a</i> (Å)	11.2391(5)
<i>b</i> (Å)	16.4848(7)
<i>c</i> (Å)	16.3761(8)
Volume (Å <sup>3</sup> )	3034.0(2)
$\beta$ (°)	90.2795(11)
<i>Z</i>	4
Temperature (K)	103
$\rho_{\text{calc}}$ (g cm <sup>-3</sup> )	1.696
$\mu$ (Mo-K $\alpha$ )/mm <sup>-1</sup>	4.267
<i>F</i> (0 0 0)	1528
Crystal size (mm)	0.28 × 0.34 × 0.40
$\lambda$ (Mo-K $\alpha$ ) (Å)	0.71073
$\theta$ ranges (°)	2.5 < $\theta$ < 31.1
Total reflection	52,497
Reflection independent ( <i>R</i> <sub>int</sub> )	9712 (0.043)
<i>h</i> / <i>k</i> / <i>l</i>	-16 : 16/ -23 : 23/ -23 : 23
Reflection observed ( <i>I</i> > 2 $\sigma$ )	8434
<i>R</i> <sub>1</sub>	0.0248
<i>WR</i> <sub>2</sub>	0.0548
Goodness of fit	1.07
$\Delta\rho_{\text{max}}$ and $\Delta\rho_{\text{min}}$ (e Å <sup>-3</sup> )	-0.93, 1.42

Note:  $R_1 = \sum ||F_o| - |F_c|| / \sum |F_o|$ ,  $wR_2 = [\sum w(F_o^2 - F_c^2)^2 / \sum w(F_o^2)]^{1/2}$ ,  $\text{Calc'd } w = 1/[\sigma^2(F_o^2) + (0.0226P)^2 + 2.1419P]$  where  $P = (F_o^2 + 2F_c^2)/3$ .

#### 2.4. Computational details

All computational studies were performed by DFT. The geometry was optimized in a closed-shell singlet (*S* = 1) state starting from the molecular structure as determined by X-ray crystallography. Here, we have assessed a group of DFT methodologies to study structural properties of the phenylimidorhenium(V) complex (**1a**) namely, functions BPV86, B3LYP, CAM-B3LYP, B3PW91, and PBEPBE in combination with basis sets LANL2DZ [33], SDD [34], LANL2 MB [33, 35], Def2-631G [36, 37], and STMIDI [38, 39]. For rhenium, the core electrons (60) were treated through the pseudo-potential approximations (ECP) as included in the LANL2DZ [33] basis set. The valence electrons for the non-metal atoms in STMIDI were treated with MIDI [38], those for the metal were described by a basis set (8s7p6d2f1g)/[6s5p3d2f1g] [34]. The core electrons were replaced by Stuttgart effective core pseudo-potentials [34, 39]. These basis sets take relativistic effects into consideration. This consideration bears some meaning specifically when systems with heavy atoms are studied [40]. TDDFT method was employed to calculate 65 singlet transitions for **1a** in dichloromethane solution [41], the latter being described by the conductor-like polarizable continuum model (C-PCM) [42, 43]. Electronic spectra were simulated by the program package GAUSSIAN 09, Rev. C.01 [44], which has been used for all the theoretical studies reported in this work. The results were interpreted and plotted using GaussSum [45] and Gabedit [46] software, respectively. For the determination of Gibbs free energy the same basis set and the same solvent model were considered.

### 3. Results and discussion

#### 3.1. Synthesis

H<sub>2</sub>L, a 1 : 1 Schiff-base condensate of ethanolamine and salicylaldehyde, was reported earlier [22, 47, 48]. **1a**, the phenylimidorhenium(V) complex under study, has been obtained by ligand exchange of *trans*-[Re(NPh)(PPh<sub>3</sub>)<sub>2</sub>Cl<sub>3</sub>] with 2-[(2-hydroxyethylimino)methyl]phenol (H<sub>2</sub>L) in equimolar proportions. **1a** has been prepared in toluene and was isolated as a solid green mass. C, H, and N micro-analytical data of the crystals of **1a** are consistent with our proposed empirical formula. **1a** is soluble in dichloromethane, chloroform, acetone, toluene, acetonitrile, DMSO, and DMF. At room temperature (298 K), **1a** is diamagnetic. **1a** is a non-electrolyte in acetonitrile solution.

#### 3.2. X-ray crystal structure

Green air-stable crystals of **1a** suitable for X-ray diffraction were obtained by slow direct diffusion of petroleum ether (40–60 °C) into a moderately concentrated solution of **1a** in dichloromethane at room temperature. An ORTEP perspective view of the asymmetric unit along with the atom numbering scheme is shown in figure 1. Selected metrical parameters are given in table 2. The rhenium is at the center of a distorted octahedral environment. The basal plane is formed by the imino nitrogen of HL<sup>-</sup>, two chlorides and PPh<sub>3</sub>. Like oxorhenium(V) [22], our ligand also binds the rhenium center in **1a** in a bidentate mode. The Re

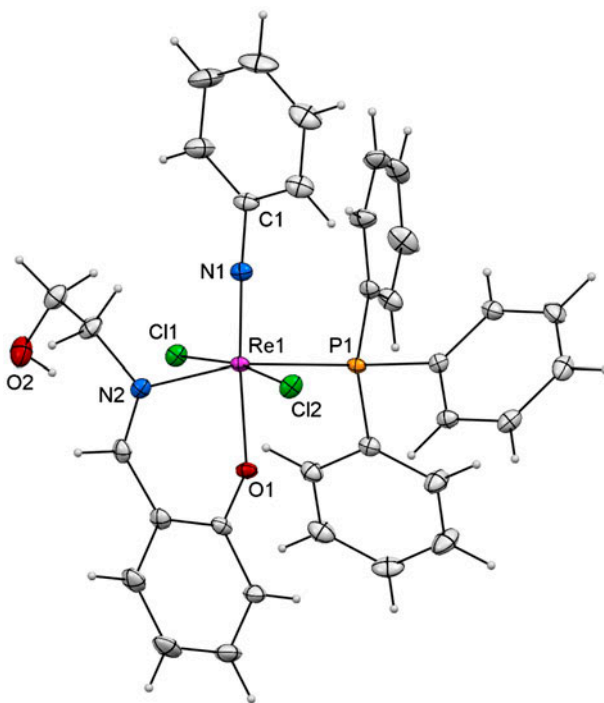


Figure 1. ORTEP diagram of **1a** showing the atom labeling scheme with 30% probability ellipsoids.

Table 2. Selected experimental bond distances (Å) and angles (°) for **1a**.

Re1–N1	1.726(2)	Re1–N2	2.126(2)
Re1–O1	1.9727(17)	Re1–P1	2.4616(6)
Re1–Cl1	2.4238(6)	Re1–Cl2	2.4066(6)
Cl1–Re1–Cl2	171.74(2)	Cl2–Re1–P1	96.22(2)
Cl1–Re1–P1	89.24(2)	Cl2–Re1–O1	85.21(5)
Cl1–Re1–O1	89.32(5)	Cl2–Re1–N1	89.73(7)
Cl1–Re1–N1	96.00(7)	Cl2–Re1–N2	82.41(6)
Cl1–Re1–N2	90.91(6)	P1–Re1–O1	82.90(5)
P1–Re1–N1	94.95(7)	O1–Re1–N1	174.25(8)
P1–Re1–N2	167.40(6)	O1–Re1–N2	84.50(7)
N1–Re1–N2	97.57(8)	Re1–N1–C1	168.94(18)

center is displaced by 0.147(3) Å towards (Re≡NPh)<sup>3+</sup> from this basal plane. The monoanionic phenolate oxygen (O1) of the ligand is *trans* to the (Re≡NPh)<sup>3+</sup>. This *trans* position of O1 is consistent with the *trans* directing influence of (Re≡NPh)<sup>3+</sup>. This is the normal mode of binding of a salicylaldimine-derived ligand regardless of its denticity [49, 50]. The Re1–N1 distance is 1.726(2) Å, in the range 1.67–1.74 Å, typical for mononuclear complexes of rhenium(V) having a [Re≡NR]<sup>3+</sup> core. This length affirms the presence of a triple bond, Re≡N [51–57]. The Re1–N1–C1 bond angle is 168.94(18)°. This value is closer to

Table 3. Bond distances (Å) of rhenium with coordinated oxygen and nitrogen and ligand bite angle (°) in some oxo/imidorhenium(V) complexes.

N, O donor ligand	[ReOCl <sub>2</sub> (N–O)PPh <sub>3</sub> ]/ [ReNArCl <sub>2</sub> (N–O)PPh <sub>3</sub> ]	Re–O <sup>a</sup>	Re–N <sup>b</sup>	∠OREN <sup>c</sup>	Ref.
bopyH = benzoylpyridine	<i>cis</i> -[ReOCl <sub>2</sub> (bopyH)(PPh <sub>3</sub> )]	1.921(4)	2.146(6)	75.0(2)	[58(a)]
hbtH = 2-(2'-hydroxyphenyl)-2-benzothiazole	<i>cis</i> -[ReOCl <sub>2</sub> (hbt)(PPh <sub>3</sub> )]	1.945(3)	2.172(3)	82.18(13)	[58(b)]
	<i>cis</i> -[ReOCl <sub>2</sub> (hbt)(PPh <sub>3</sub> )]	1.939(7)	2.173(9)	81.9(3)	
	<i>cis</i> -[ReOCl <sub>2</sub> (hmpbta)(PPh <sub>3</sub> )]	1.9458(18)	2.155(2)	80.34(8)	
Hhpb = 2-(2-hydroxyphenyl)-1 <i>H</i> -benzimidazole	<i>trans</i> [ReOCl <sub>2</sub> (hpb)(PPh <sub>3</sub> )]	1.940(4)	2.146(5)	81.10(19)	[58(c)]
	<i>cis</i> -[ReOCl <sub>2</sub> (hpb)(PPh <sub>3</sub> )]	1.953(2)	2.120(3)	81.38(10)	
HhqN = 8-hydroxyquinoline	<i>cis</i> -[ReOCl <sub>2</sub> (hqN)(PPh <sub>3</sub> )]	1.997(4)	2.148(4)	87.0(2)	[58(d)]
Hhep = 2-pyridine-ethanol	[ReOCl <sub>2</sub> (hep)(PPh <sub>3</sub> )]	1.868(2)	2.200(2)	86.0(1)	
H <sub>2</sub> map = 2-aminobenzyl alcohol	[ReOCl <sub>2</sub> (Hmap)(PPh <sub>3</sub> )]	1.861(8)	2.158(9)	80.0(3)	[58(e)]
Hbcp = N-(2-hydroxybenzylidene)-benzothiazole	<i>cis</i> -[Re(bcp)OCl <sub>2</sub> (PPh <sub>3</sub> )]	1.949(5)	2.165(6)	82.8(2)	[58(f)]
APOH = 4-anilino-3-penten-2-one	<i>trans</i> [ReO(APO)Cl <sub>2</sub> (PPh <sub>3</sub> )]	2.002(2)	2.105(2)	83.50(8)	[49]
DPOH = 4-[2,6-dimethylanilino]-3-penten-2-one	<i>trans</i> [ReO(DPO)Cl <sub>2</sub> (PPh <sub>3</sub> )]	2.010(3)	2.124(3)	82.8(1)	[49]
HL <sup>1</sup> P = Ph <sub>2</sub> PC <sub>6</sub> H <sub>4-2</sub> -HC=N (C <sub>6</sub> H <sub>4-2</sub> -OH)	<i>cis</i> -[ReOCl <sub>2</sub> (PPh <sub>3</sub> )(L <sup>1</sup> PO)]	1.958(6)	2.192(7)	76.3(3)	[59(d)]
HL = 2-allylimino- methylphenol	<i>cis</i> -[ReOCl <sub>2</sub> (L)(PPh <sub>3</sub> ) <sub>2</sub> ]	1.930(3)	2.134(5)	83.14(15)	[64]
H <sub>2</sub> L = 2-[(2-hydroxyethyl imino) methyl] phenol	<i>cis</i> -[ReOCl <sub>2</sub> (HL)(PPh <sub>3</sub> )]	1.941(2)	2.130(3)	82.54(12)	[22]
	<i>trans</i> [Re(NPh)(HL)(PPh <sub>3</sub> )Cl <sub>2</sub> ]	1.9727(17)	2.126(2)	84.50(7)	This work
hmbzim = 2-hydroxymethyl benzimidazole	<i>cis</i> -[Re( <i>p</i> -NC <sub>6</sub> H <sub>4</sub> CH <sub>3</sub> )Cl <sub>2</sub> (hmbzim)(PPh <sub>3</sub> )]	2.009(8)	2.120(11)	76.9(4)	[67]

<sup>a</sup>Bond length of Re and ligand O.

<sup>b</sup>Bond length of Re and ligand N.

<sup>c</sup>Ligand bite angle; *cis*–*cis*-Cl, Cl; *trans* – *trans* Cl, Cl.



180° rather than 120°. Thus, the X-ray data hints at *sp* hybridization of the N1 donor. In table 3, we have compared the Re–O, Re–N and the bite angle ( $\angle\text{OReN}$ ) of our compound with other analogous oxo-, imido- Re(V) systems with N/O donor bidentate chelating ligands of the type  $[\text{ReOCl}_2(\text{N}-\text{O})\text{PPh}_3]$  and  $[\text{ReNArCl}_2(\text{N}-\text{O})\text{PPh}_3]$ . It appears that the Re–O and Re–N bond lengths are 1.861(8)–2.013(3) and 2.105(2)–2.200(2) Å, respectively. In our case, the corresponding bond distances are also in the stipulated range. In **1a**, the Re1–O1 and Re1–N2 distances are 1.9727(17) and 2.126(2) Å. The bite angle in **1a** also matches available literature [75.0(2)–87.0(2)] (table 3). The N1–Re1–O1 angle of 174.25 (8)° is in considerable deviation from the idealized value 180° for a regular octahedral geometry. Consequently, the narrow bite angle [O1–Re1–N2 84.50(7)°] of the chelating ligand in **1a** significantly distorts the octahedral geometry around the rhenium center in a ‘N<sub>2</sub>OCl<sub>2</sub>P’ coordination environment. The majority of the known imidorhenium(V) complexes, based on salicylaldimine ligands, display structures with halides in *trans* dispositions [59–62]; **1a** is not an exception. The Cl(1)–Re1–Cl(2) angle is 171.74(2)°, near 180°. Thus, **1a** is a *trans*-Cl,Cl complex with the Re–Cl bond lengths of 2.4238(6) and 2.4066(6) Å.

The crystal structure is stabilized by CH– $\pi$  hydrogen bonds. In **1a**, the distance between the methylene proton (H15A) and the center of the phenyl ring (comprising C22, C23, C24, C25, C26, and C27) in PPh<sub>3</sub> of another molecule is 2.785 Å and the distance between C15 and the center of the phenyl ring is 3.701 Å. These distances are optimum for significant CH/ $\pi$  interactions [63, 64].

### 3.3. Geometry optimization

Optimization starting from the crystallographically determined molecular structure of **1a** leads to a minimum as stationary point. The general features observed in the experimental data are well-reproduced in the calculations, despite a few large deviations in calculated bond lengths and angles. All the methods attempted give acceptable discrepancies between the experimental and theoretical geometric data (table S1, see online supplemental material at <http://dx.doi.org/10.1080/00958972.2014.996145>). The Re1–N1 and other coordinating bonds with rhenium are sensitive parameters for the basis sets and functionals of DFT under study. The calculated Re1–N1 bond length for **1a** is 1.723–1.796 Å (experimental value 1.726(2) Å). The differences in Re1–N1 bond distances between calculated values (as obtained by employing different DFT methods) and the crystallographic result for **1a** are plotted in figure S1. From the plot, it is obvious that the best calculated result was obtained with CAM-B3LYP in combination with basis sets LANL2DZ. All other methodologies are less effective for the Re1–N1 bond length. The functional CAM-B3LYP in combination with any basis set is a judicious choice for **1a**. Similarly, the differences in the bond distances of all the bonds between calculated values (as obtained by employing several basis sets in combination with CAM-B3LYP methods) and the crystallographic results for **1a** are plotted in figure S2. For all existing bonds with the rhenium center in **1a** (Re1–N1, Re1–Cl1, Re1–Cl2, Re1–O1, Re1–N2, and Re1–P1), the data generated by the STMIDI in combination with CAM-B3LYP method can best reproduce the experimental results. Hence, we have used CAM-B3LYP in combination with STMIDI method of DFT for the prediction of the vibrational spectrum, assessments of molecular electronic structures and free energy calculations for the evaluation of redox potential for **1a**.



To elucidate the bonding properties of the *trans*-Cl,Cl **1a** isomer and *cis*-Cl,Cl **1b** isomer, calculations at the level of DFT were undertaken. The geometries were optimized in singlet state using the STMIDI with the CAM-B3LYP functional. From geometry optimization, it was found that the *trans*-Cl,Cl **1a** isomer is more stable than the *cis*-Cl,Cl **1b** isomer by 21.6 kcal M<sup>-1</sup>. Thus, the theoretical outcome corroborates our experimental findings.

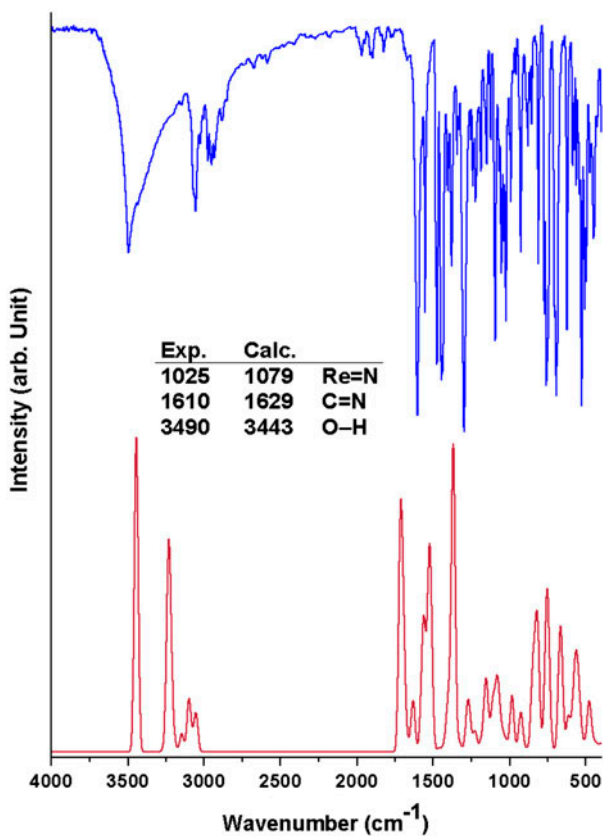
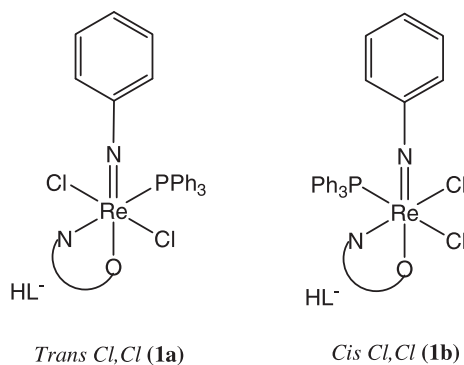


Figure 2. The experimental (blue) and calculated (red, non-scaled) vibrational spectra of **1a** (see <http://dx.doi.org/10.1080/00958972.2014.996145> for color version).

### 3.4. Spectroscopic properties

**3.4.1. FTIR and  $^1\text{H}$  NMR spectroscopy.** A very strong band at  $1610\text{ cm}^{-1}$  in the IR spectrum of **1a** is assigned to the azomethine ( $>\text{C}=\text{N}-$ ) group vibration. The IR spectrum of **1a** exhibits a sharp band at  $1025\text{ cm}^{-1}$ , assignable to the characteristic stretching frequency of  $\nu(\text{Re}\equiv\text{N})$  [13, 26]. The calculated strong stretching frequency of  $\nu(\text{Re}\equiv\text{N})$  appears at  $1079\text{ cm}^{-1}$  for **1a** and two very weak frequencies at  $1430$  and  $1564\text{ cm}^{-1}$  are also observed [13]. The experimental vibrational spectrum of **1a** has been compared with the calculated (non-scaled) one in figure 2. The calculated vibrational spectrum of **1a** is in good agreement with the experimental data. The experimental and calculated IR spectra of **1a** are similar in terms of their band positions, band intensities, and shapes. The calculated  $\nu(\text{Re}\equiv\text{N})$  and  $\nu(\text{C}=\text{N})$  frequencies for **1a** are higher than the corresponding experimental values by only  $\sim 1$  and  $\sim 5\%$ . However, these discrepancies are justified when seen from a theoretical perspective. Often, the computed gas phase data are at variance with the experimental one [65, 66].

The characteristics of all the spectral signals in the  $^1\text{H}$  NMR spectrum of **1a** are akin to the  $^1\text{H}$  NMR spectral pattern of  $\text{H}_2\text{L}$  [22] with downfield shifts. The observed signals corresponding to methylene protons are assigned at 4.01 and 4.09 ppm. The signal at 8.38 ppm indicates the imino-methine  $-\text{CH}=\text{N}-$  group in the ligand. The aromatic region is dominated by signals of triphenylphosphine protons. This region is considerably overlapped due to proton resonances arising from the phenylimido group and salicylaldimine ring.

**3.4.2. Molecular orbital description.** The partial molecular orbital energy diagrams derived from the CAM-B3LYP in combination with STMIDI calculation as well as contours of the selected frontier orbitals (HOMO–LUMO) are shown, respectively, in figures 3 and 4 for **1a**. The analyses of MOs are helpful to gain insights into the chemical bonding between rhenium and the surrounding ligands and for the understanding of the electronic properties. The electronic transitions, characters of MOs and oscillator strengths for **1a** obtained with the CAM-B3LYP in combination with STMIDI methodology are presented in table 4. The strong  $\sigma$ - and  $\pi$ -donor properties of the phenylimido ligand destabilize the  $5d_{x^2-y^2}$  and the  $5d_{yz/xz}$  orbitals within the  $d$  orbital manifold. Our calculations reproduce the rhenium  $d$  orbital manifold resulting from the presence of a terminal phenylimido ligand [13, 67, 68]. The rhenium center in **1a** is a  $5d^2$  electronic configuration. These electrons reside in an MO with a significant contribution from the  $d_{xy}$  orbital to give a singlet ground state. The HOMO to LUMO energy gap is 5.719 eV for **1a**. In **1a**, the highest occupied molecular orbital (HOMO) enjoys significant metal character, predominantly  $d_{xy}$  and bonding p orbitals of chloride. The highly populated orbitals (HOMO-2, HOMO-5, HOMO-6, HOMO-7, and HOMO-9) are mostly contributed by  $\text{PPh}_3$  orbitals. The MOs, HOMO-1, HOMO-4, and HOMO-8 predominantly exhibit the  $\pi$ -bond character of  $\text{H}_2\text{L}$  orbitals. The LUMO, LUMO + 1, LUMO + 2, LUMO + 4, LUMO + 5 orbitals are, respectively, composed of  $d_{x^2-y^2}$ ,  $d_{xz}$ ,  $d_{yz}$ ,  $d_z^2$ , and  $d_z^2$  rhenium orbitals in antibonding arrangements. In contrast, the LUMO + 3 is mainly contributed by the  $\pi$ -antibonding orbitals of  $\text{PPh}_3$ . The MOs of HOMO-3 are mainly influenced by the  $\pi$ -bond character of phenylimido ligand (NPh), while the LUMO and LUMO + 1 are predominantly contributed by the  $\pi$ -antibonding orbitals.

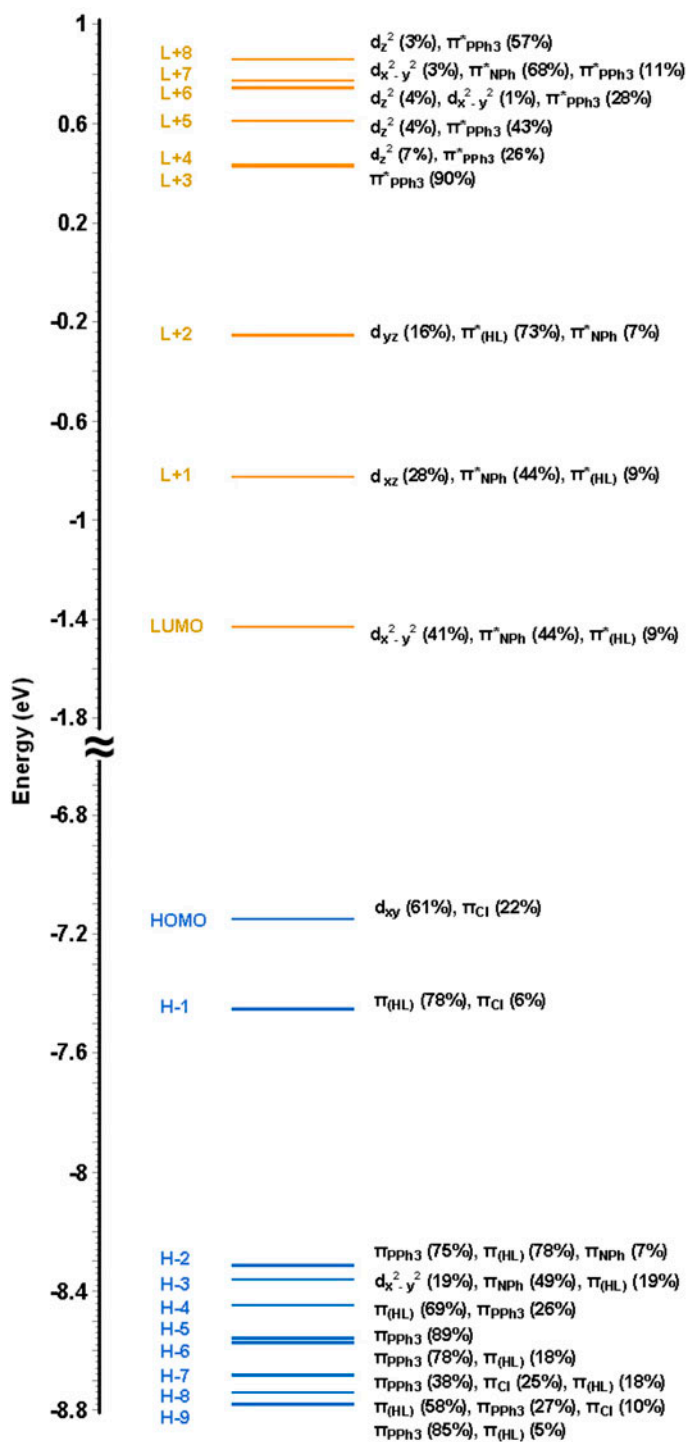


Figure 3. The MO diagram of **1a** showing the character and energy (eV).

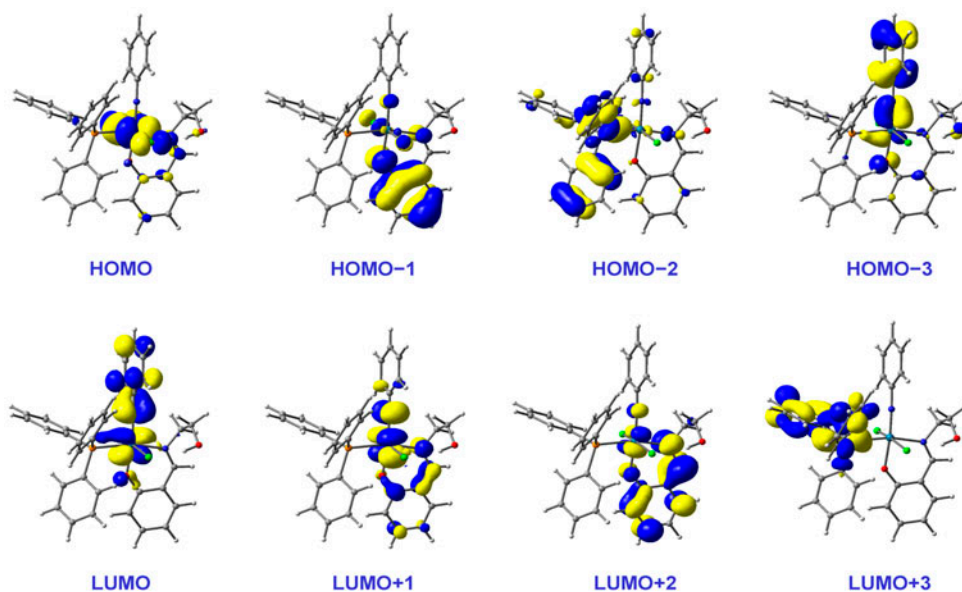


Figure 4. Selected HOMOs and LUMOs of **1a**. Positive values of the orbital contour are represented in yellow (0.04 au) and negative values in blue (-0.04 au) (see <http://dx.doi.org/10.1080/00958972.2014.996145> for color version).

Table 4. Calculated electronic transitions of **1a** in dichloromethane employing the STMIDI-CAM-B3LYP method.

Most important orbital excitations	$\lambda$	$f$	Experimental $\lambda$ ( $\epsilon$ )
H $\rightarrow$ L	640.61	0.0001	714 (84)
H $\rightarrow$ L+1	572.54	0.0001	555 (118)
			423 (3260)
H-1 $\rightarrow$ L	361.88	0.004	360 (12,295)
H $\rightarrow$ L+4, H $\rightarrow$ L+5	358.50	0.002	
H-1 $\rightarrow$ L+1, H $\rightarrow$ L+2	326.16	0.029	319 (19,526)
H-10 $\rightarrow$ L, H-7 $\rightarrow$ L	312.78	0.040	
H-3 $\rightarrow$ L, H-10 $\rightarrow$ L, H-7 $\rightarrow$ L	302.39	0.221	
H $\rightarrow$ L+2, H-1 $\rightarrow$ L+1	291.36	0.317	
H-2 $\rightarrow$ L, H-1 $\rightarrow$ L+2	281.37	0.208	
H-2 $\rightarrow$ L+1, H-13 $\rightarrow$ L+1, H-4 $\rightarrow$ L	256.44	0.062	263 (25,400)
H-4 $\rightarrow$ L, H-12 $\rightarrow$ L	255.64	0.033	
H-10 $\rightarrow$ L+1, H-7 $\rightarrow$ L+1, H-12 $\rightarrow$ L	251.04	0.189	

Note:  $\lambda$  wavelength (nm);  $\epsilon$  molar absorption coefficient ( $\text{dm}^3 \text{mol}^{-1} \text{cm}^{-1}$ );  $f$  oscillator strength; H highest occupied molecular orbital; L lowest unoccupied molecular orbital.

**3.4.3. Electronic spectra.** The absorption spectrum of **1a** is simulated in the presence of dichloromethane employing the TDDFT with the CAM-B3LYP in combination with STMIDI method. The outcome is in agreement with our experimental data (figure 5). Calculated spin-allowed singlet-singlet electronic transitions of **1a** along with the experimental data are summarized in table 4. Only transitions with oscillator strengths higher than 0.0200 are taken into consideration for the high energy part (360–251 nm) of the spectrum of **1a**. The calculated low-energy absorption bands at 640.61 and 572.54 nm for **1a** are contributed

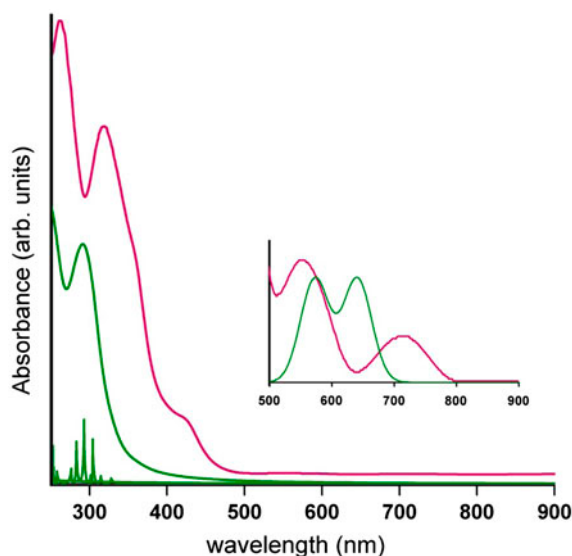


Figure 5. The experimental (red) and calculated (green) electronic absorption spectra of **1a** and the magnified part is in the inset (see <http://dx.doi.org/10.1080/00958972.2014.996145> for color version).

by HOMO  $\rightarrow$  LUMO and HOMO  $\rightarrow$  LUMO + 1 transitions. Analyses of the orbitals also allow us to decipher the types of transitions. These transitions can best be described as mixed  $d \rightarrow d$  (ligand field; LF),  $d\pi_{(\text{Cl})} \rightarrow d_{\text{Re}}$  (ligand–metal charge transfer; LMCT), and  $\pi_{(\text{Cl})} \rightarrow \pi^*_{(\text{NPh})}/\pi^*_{(\text{HL})}$  (ligand–ligand charge transfer; LLCT) or may be delocalized metal ligand–ligand charge transfer; MLLCT transitions. The above bands are correlated with the experimentally determined bands at 714 and 555 nm. The absorption band calculated at 361.88 nm (observed at 360 nm) is assigned to HOMO-1  $\rightarrow$  LUMO transition. The origin of this transition can be mixed  $\pi_{(\text{Cl})} \rightarrow d_{\text{Re}}$ ,  $d_{(\text{HL})} \rightarrow \pi^*_{(\text{NPh})}/\pi^*_{(\text{HL})}$  or  $\pi_{(\text{Cl})} \rightarrow \pi^*_{(\text{HL})}/\pi^*_{(\text{NPh})}$  excitation. Intense bands in the high energy region are largely due to LLCT transitions [13].

### 3.5. Electrochemistry

The redox properties of **1a** have been examined in dichloromethane at GC electrode under  $\text{N}_2$ . **1a** exhibits a redox couple on the positive side of the Ag/AgCl reference electrode. The CV of **1a** (figure 6) shows a quasi-reversible voltammogram at 1.128 V *versus* Ag/AgCl reference electrode. The corresponding peak current ratio,  $i_{\text{pa}}/i_{\text{pc}}$ , is 1.05 with peak-to-peak separation,  $\Delta E$  of 114 mV.  $\text{H}_2\text{L}$  is electrochemically inert in the potential range of interest, i.e. on the positive side of Ag/AgCl. Thus, this oxidation can be assigned as metal centered. Comparison of the voltammetric peak currents with those of the ferrocene–ferrocenium couple under the same experimental conditions establishes that the oxidative response in **1a** involves one electron, ascribed to the  $\text{Re}^{(\text{VI})}/\text{Re}^{(\text{V})}$  couple [69–72]. The electrochemical data for **1a** are tabulated in table 5. The peak current,  $i_{\text{p}}$ , increases with the square root of scan rate ( $v^{1/2}$ ), but not in proportionality. Thus, the metal centered oxidation for **1a** is quasi-reversible [71]. The electrochemical response for **1a** can be assigned as:

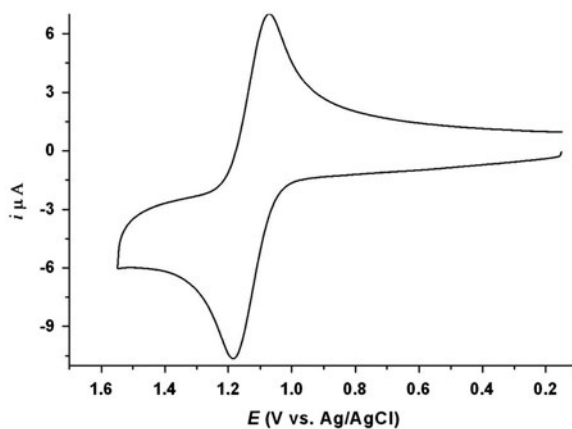


Figure 6. Cyclic voltammogram of **1a** in dichloromethane at a scan rate of  $100 \text{ mV s}^{-1}$ . The analyte concentration was  $1.012 \times 10^{-3} \text{ M}$ .

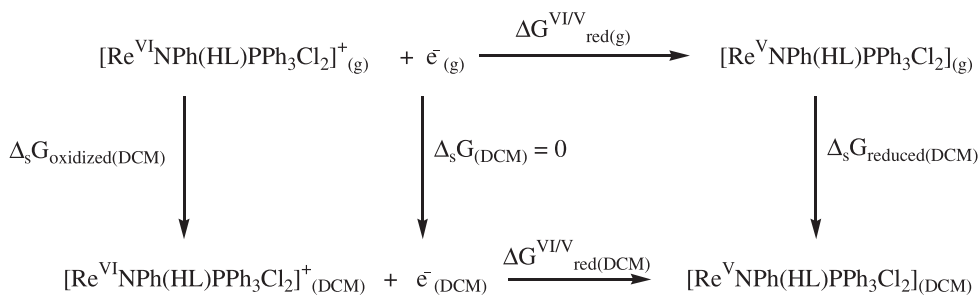
Table 5. Cyclic voltammetric data for **1a**.

$E_{\text{pa}}(i_{\text{pa}})$	$E_{\text{pc}}(i_{\text{pc}})$	$\Delta E$	$i_{\text{pa}}/i_{\text{pc}}$	$E_{1/2}$ (Exp.)	$E$ (Theo.)
1.185(8.57)	1.071(8.16)	114	1.05	1.128	1.186

$sE_{\text{pa}}$  = anodic peak potential, V;  $E_{\text{pc}}$  = cathodic peak potential, V;  $i_{\text{pa}}$  = anodic peak current,  $\mu\text{A}$ ;  $i_{\text{pc}}$  = cathodic peak current,  $\mu\text{A}$ ;  $E_{1/2} = 0.5(E_{\text{pc}} + E_{\text{pa}})$  V;  $\Delta E = E_{\text{pa}} - E_{\text{pc}}$ , mV.



The electrochemical behavior of **1a** can be rationalized through DFT calculations [73]. The contribution of rhenium to the occupied MOs is significant. Thus, **1a** shows predominant metal-based oxidation. This enables us to determine the Gibbs free energy theoretically, which in turn leads to prediction of reduction free energy of **1a**. In doing so, a Born-Haber thermodynamic cycle was framed. The free energies of the oxidized as well as the reduced forms of **1a** in the gas phase and also in solution (scheme 1) were incorporated in this



Scheme 1. Proposed thermodynamic cycle for the prediction of reduction free energy ( $\Delta G^{\text{VI/V}}_{\text{red}}$ ).

cycle. The estimated reduction free energy was then referenced with respect to standard hydrogen electrode (SHE).

From the above cycle, we can set the following equations:

$$\Delta G_{\text{red(DCM)}}^{\text{VI/V}} = \Delta G_{\text{red(g)}}^{\text{VI/V}} + \Delta \Delta G_{\text{solv}} \quad (2a)$$

$$\Delta \Delta G_{\text{solv}} = \Delta_s G_{\text{reduced(DCM)}} - \Delta_s G_{\text{oxidized(DCM)}} \quad (2b)$$

$$\Delta G_{\text{red}} = \Delta G_{\text{red(DCM)}}^{\text{VI/V}} - \Delta G_{\text{red}}^{\text{Ref. electrode}} \quad (2c)$$

Here,  $\Delta G_{\text{red(g)}}^{\text{VI/V}}$  is the reduction free energy of **1a** in the gas phase.  $\Delta_s G_{\text{reduced(DCM)}}$  and  $\Delta_s G_{\text{oxidized(DCM)}}$ , respectively, are the solvation free energies of the reduced and oxidized forms of **1a**.  $\Delta G_{\text{solv}}$  is the difference between the solvation free energies of the reduced and the oxidized complexes, i.e.  $(\Delta_s G_{\text{reduced(DCM)}} - \Delta_s G_{\text{oxidized(DCM)}})$ . The absolute reduction free energy for Re(VI) to Re(V),  $\Delta G_{\text{red(DCM)}}^{\text{VI/V}}$ , was determined by using equations (2a) and (2b). Subsequently, equation (2c) was used to obtain the reduction free energy of a reference electrode. The reference electrode considered here for the sake of computation is the standard hydrogen electrode (SHE). In our present calculation, the absolute reduction free energy of SHE was taken as 4.44 eV, as recommended by IUPAC for the absolute value of SHE in 1986 by Trasatti et al. [74]. The reduction potential value was evaluated from the pre-determined  $\Delta G_{\text{red}}$  employing the standard relationships,  $E_{1/2} = -\Delta G_{\text{red}}/(nF)$  where  $n$  is the number of electrons transferred and  $F$  is the Faraday constant [75]. We have determined the reduction free energy ( $\Delta G_{\text{red(DCM)}}^{\text{VI/V}}$ ) through DFT by using the solvent model, C-PCM and the obtained value is 5.835 eV. In our present exercise, the calculated  $E_{1/2}$  is 1.395 V *versus* SHE. After necessary reference conversion, this value comes out as 1.186 V *versus* Ag/AgCl. Thus the theoretical outcome reasonably corroborates our experimental redox potential, 1.128 V *versus* Ag/AgCl. We also compare our determined potential with the experimental value of a system previously reported. The  $\text{Re}^{(\text{VI})}/\text{Re}^{(\text{V})}$  redox potential of a Re(V)-oxo compound,  $[\text{Re}^{\text{V}}\text{O}(\text{HL})\text{PPh}_3\text{Cl}_2]$ , was found to be 1.420 V *versus* Ag/AgCl [22]. Clearly, this value is higher than that found in **1a** under identical electrochemical situation. Most likely, this is due to the structural difference between  $[\text{Re}^{\text{V}}\text{O}(\text{HL})\text{PPh}_3\text{Cl}_2]$  and  $[\text{Re}^{\text{V}}\text{NPh}(\text{HL})\text{PPh}_3\text{Cl}_2]$ , rendering **1a** electrochemically more labile than the Re(V)-oxo system. Thus, the  $\text{Re}^{(\text{VI})}/\text{Re}^{(\text{V})}$  redox potential is less here.

#### 4. Conclusion

We have synthesized and characterized a new phenylimidorhenium(V) complex from an ancillary ligand, 2-[(2-hydroxyethylimino)methyl]phenol ( $\text{H}_2\text{L}$ ). The X-ray crystal structure of  $[\text{Re}(\text{NPh})(\text{HL})(\text{PPh}_3)\text{Cl}_2]$  (**1a**) reveals that the rhenium(V) center is octahedral 'N<sub>2</sub>OPCl<sub>2</sub>'. The two chlorides are *trans* to each other. Thus, **1a** can best be described as a *trans*-Cl,Cl phenylimidorhenium(V) complex. DFT calculations in the gas phase reveal that *trans*-Cl,Cl phenylimidorhenium(V), **1a** is more stable than the *cis* counterpart, *cis*-Cl,Cl phenylimidorhenium(V) complex, **1b** by 21.60 kcal M<sup>-1</sup>. The electronic structure of **1a** has also been studied by C-PCM solvent model (dichloromethane) employing DFT level of theory and the outcomes agree with the experimental data. In CV, **1a** undergoes a quasi-reversible one



electron oxidation from Re(V) to Re(VI) in dichloromethane at 1.128 V *versus* Ag/AgCl. The redox potential was also modeled through DFT. The calculated potential, 1.186 V *versus* Ag/AgCl corroborates our experimental redox potential, 1.128 V *versus* Ag/AgCl.

## Supplementary material

Crystallographic data for the structural analyses have been deposited with the Cambridge Crystallographic Data Center (CCDC No. 975550). Copies of this information can be obtained free of charge from the Director, CCDC, 12 Union Road, Cambridge CB2 1EZ, UK (Fax: +44 1223336033; E-mail: [deposit@ccdc.cam.ac.uk](mailto:deposit@ccdc.cam.ac.uk) or www: <http://www.ccdc.cam.ac.uk>). Supplementary data associated with this article can be found in the online version.

## Acknowledgements

Financial support (F. No. SR/FT/CS-75/2010) received from the SERB under Department of Science and Technology (DST), India, is gratefully acknowledged. J.P. Naskar gratefully acknowledges the University Grants Commission (UGC), New Delhi, India for financial support [F. No. 41-220/2012 (SR)].

## References

- [1] M. Gielen, E.R.T. Tiekink (Eds.). *Metallotherapeutic Drugs and Metal-based Diagnostic Agents: The Use of Metals in Medicine*, John Wiley & Sons, Sussex, England (2005).
- [2] W.A. Volkert, T.J. Hoffman. *Chem. Rev.*, **99**, 2269 (1999).
- [3] L. Hansen, R. Cini, A.J. Taylor, L.G. Marzilli. *Inorg. Chem.*, **31**, 2801 (1992).
- [4] P.J. Blower, A.S.K. Lam, M.J. O'Doherty, A.G. Kettle, Anthony J. Coakley Jr. *Eur. J. Nucl. Med.*, **25**, 613 (1998).
- [5] P.J. Blower, A.G. Kettle, M.J. O'Doherty, A.J. Coakley, F.F. Knapp Jr. *Eur. J. Nucl. Med.*, **27**, 1405 (2000).
- [6] S. Prakash, M.J. Went, P.J. Blower. *Nucl. Med. Biol.*, **23**, 543 (1996).
- [7] S. Guhlke, A. Schaffland, P.O. Zamora, J. Sartor, D. Diekmann, H. Bender, F.F. Knapp, H.J. Biersack. *Nucl. Med. Biol.*, **25**, 621 (1998).
- [8] C.-B. Liu, G.-Z. Liu, N. Liu, Y.-M. Zhang, J. He, M. Rusckowski, D.J. Hnatowich. *Nucl. Med. Biol.*, **30**, 207 (2003).
- [9] C.C. Romão, F.E. Kühn, W.A. Herrmann. *Chem. Rev.*, **97**, 3197 (1997).
- [10] J.H. Espenson. *Coord. Chem. Rev.*, **249**, 329 (2005).
- [11] Y. Miyashita, T. Ohashi, A. Imai, N. Amir, K. Fujisawa, K. Okamoto. *Sci. Technol. Adv. Mater.*, **6**, 660 (2005).
- [12] G.S. Owens, J. Arias, M.M. Abu-Omar. *Catal. Today*, **55**, 317 (2000).
- [13] B. Machura, I. Gryca, J.G. Małecki, F. Alonso, Y. Moglie. *J. Chem. Soc., Dalton Trans.*, 2596 (2014).
- [14] W. Maniukiewicz, M. Bukowska-Strzyżewska. *J. Chem. Crystallogr.*, **26**, 43 (1996).
- [15] C. Boskovic, E. Rusanov, H. Stoeckli-Evans, H.U. Güdel. *Inorg. Chem. Commun.*, **5**, 881 (2002).
- [16] N. Hoshino, T. Ito, M. Nihei, H. Oshio. *Inorg. Chem. Commun.*, **6**, 377 (2003).
- [17] Y.M. Chumakov, B.Y. Antosyak, V. Tsapkov, G. Bocelli, A.P. Gulya. *Koord. Khim.*, **30**, 486 (2004).
- [18] M. Dey, C.P. Rao, P.K. Saarenketo, K. Rissanen. *Inorg. Chem. Commun.*, **5**, 924 (2002).
- [19] N. Hoshino, T. Ito, M. Nihei, H. Oshio. *Inorg. Chem. Commun.*, **5**, 844 (2002).
- [20] A. Sieber, C. Boskovic, R. Bircher, O. Waldmann, S.T. Ochsenein, G. Chaboussant, H.U. Güdel, N. Kirchner, J. van Slageren, W. Wernsdorfer, A. Neels, H. Stoeckli-Evans, S. Janssen, F. Juranyi, H. Mutka. *Inorg. Chem.*, **44**, 4315 (2005).
- [21] K. Van Hecke, P. Nockemann, K. Binnemans, L. Van Meervelt. *Acta Crystallogr. Sect. E*, **63**, m569 (2007).
- [22] S. Majumder, J.P. Naskar, S. Banerjee, A. Bhattacharya, P. Mitra, S. Chowdhury. *J. Coord. Chem.*, **66**, 1178 (2013).
- [23] W. Koch, M.C. Holthausen. *A Chemist's Guide to Density Functional Theory*, 2nd Edn, Wiley-VCH Verlag GmbH, New York, NY (2001).

- [24] J.S. Gancheff, P.A. Denis, F. Ekkehardt Hahn. *J. Mol. Struct. (Theochem.)*, **941**, 1 (2010).
- [25] J.S. Gancheff, Álvaro Acosta, D. Armentano, G. De Munno, R. Chiozzone, R. González. *Inorg. Chim. Acta*, **387**, 314 (2012).
- [26] I. Gryca, B. Machura, J.G. Malecki, L.S. Shul'pina, A.J.L. Pombeiro, G.B. Shul'pin. *J. Chem. Soc., Dalton Trans.*, 5759 (2014).
- [27] M. Wolff, L. Munoz, A. François, C. Carrayon, A. Seridi, N. Saffon, C. Picard, B. Machura, E. Benoist. *J. Chem. Soc., Dalton Trans.*, 7019 (2013).
- [28] J.S. Gancheff, P.A. Denis, F.E. Hahn. *Spectrochim. Acta, Part A*, **76**, 348 (2010).
- [29] G.A. Rowe, J. Chatt. *J. Chem. Soc.*, 4019, (1962).
- [30] SAINT Plus. *Data Reduction and Correction Program (Version 6.01)*, Bruker AXS, Madison, WI (1998).
- [31] SADABS v.2.01. *Bruker/Siemens Area Detector Absorption Correction Program*, Bruker AXS, Madison, WI (1998).
- [32] G.M. Sheldrick. *Acta Crystallogr. Sect. A*, **64**, 112 (2008).
- [33] P.J. Hay, W.R. Wadt. *J. Chem. Phys.*, **82**, 299 (1985).
- [34] (a) M. Dolg, U. Wedig, H. Stoll, H. Preuss. *J. Chem. Phys.*, **86**, 866 (1987); (b) J.M.L. Martin, A. Sundermann. *J. Chem. Phys.*, **114**, 3408 (2001); (c) D. Andrae, U. Häussermann, M. Dolg, H. Stoll, H. Preuss. *Theor. Chim. Acta*, **77**, 123 (1990).
- [35] P.J. Hay, W.R. Wadt. *J. Chem. Phys.*, **82**, 270 (1985).
- [36] D. Rappoport, F. Furche. *J. Chem. Phys.*, **133**, 134105 (2010).
- [37] (a) W.J. Hehre, R. Ditchfield, J.A. Pople. *J. Chem. Phys.*, **56**, 2257 (1972); (b) M.M. Francl, W.J. Pietro, W.J. Hehre, J.S. Binkley, M.S. Gordon, D.J. DeFrees, J.A. Pople. *J. Chem. Phys.*, **77**, 3654 (1982).
- [38] R.E. Easton, D.J. Giesen, A. Welch, C.J. Cramer, D.G. Truhlar. *Theor. Chim. Acta*, **93**, 281 (1996).
- [39] A. Bergner, M. Dolg, W. Küchle, H. Stoll, Heinzwerner Preuß. *Mol. Phys.*, **80**, 1431 (1993).
- [40] P. Pyykkö. *The Effect of Relativity in Atoms, Molecules and The Solid State*, Plenum, New York, NY (1990).
- [41] E.S. Böes, P.R. Livotto, H. Stassen. *Chem. Phys.*, **331**, 142 (2006).
- [42] V. Barone, M. Cossi. *J. Phys. Chem. A*, **102**, 1995 (1998).
- [43] M. Cossi, N. Rega, G. Scalmani, V. Barone. *J. Comput. Chem.*, **24**, 669 (2003).
- [44] M.J. Frisch, G.W. Trucks, H.B. Schlegel, G.E. Scuseria, M.A. Robb, J.R. Cheeseman, G. Scalmani, V. Barone, B. Mennucci, G.A. Petersson, H. Nakatsuji, M. Caricato, X. Li, H.P. Hratchian, A.F. Izmaylov, J. Bloino, G. Zheng, J.L. Sonnenberg, M. Hada, M. Ehara, K. Toyota, R. Fukuda, J. Hasegawa, M. Ishida, T. Nakajima, Y. Honda, O. Kitao, H. Nakai, T. Vreven, J.A. Montgomery Jr, J.E. Peralta, F. Ogliaro, M. Bearpark, J.J. Heyd, E. Brothers, K.N. Kudin, V.N. Staroverov, R. Kobayashi, J. Normand, K. Raghavachari, A. Rendell, J.C. Burant, S.S. Iyengar, J. Tomasi, M. Cossi, N. Rega, J.M. Millam, M. Klene, J.E. Knox, J.B. Cross, V. Bakken, C. Adamo, J. Jaramillo, R. Gomperts, R.E. Stratmann, O. Yazyev, A.J. Austin, R. Cammi, C. Pomelli, J.W. Ochterski, R.L. Martin, K. Morokuma, V.G. Zakrzewski, G.A. Voth, P. Salvador, J.J. Dannenberg, S. Dapprich, A.D. Daniels, Ö. Farkas, J.B. Foresman, J.V. Ortiz, J. Cioslowski, D.J. Fox. *GAUSSIAN 09, Revision C.01*, Gaussian, Inc., Wallingford, CT (2009).
- [45] N.M. O'boyle, A.L. Tenderholt, K.M. Langner. *J. Comput. Chem.*, **29**, 839 (2008).
- [46] A.-R. Allouche. *J. Comput. Chem.*, **32**, 174 (2011).
- [47] T. Głowiak, L. Jerzykiewicz, J.M. Sobczak, J.J. Ziótkowski. *Inorg. Chim. Acta*, **356**, 387 (2003).
- [48] M. Dey, C.P. Rao, P. Saarenketo, K. Rissanen, E. Kolehmainen. *Eur. J. Inorg. Chem.*, **2002**, 2207 (2002).
- [49] A. Sachse, N.C. Mösch-Zanetti, G. Lyashenko, J.W. Wielandt, K. Most, J. Magull, F.D. Dall'Antonia, A. Pal, R. Herbst-Irmer. *Inorg. Chem.*, **46**, 7129 (2007).
- [50] T.I.A. Gerber, D. Luzipo, P. Mayer. *Inorg. Chim. Acta*, **357**, 429 (2004).
- [51] L. Wei, J. Babich, J.W. Zubieta. *Inorg. Chem.*, **43**, 6445 (2004).
- [52] G. Bandoli, T.I.A. Gerber, J. Perils, J.G.H. du Preez. *Inorg. Chim. Acta*, **278**, 96 (1998).
- [53] I. Booyens, T.I.A. Gerber, E. Hosten, P. Mayer. *J. Coord. Chem.*, **60**, 1749 (2007).
- [54] J.B. Arterburn, K.V. Rao, D.M. Goreham, M.V. Valenzuela, M.S. Holguin, K.A. Hall, K.C. Ott, J.C. Bryan. *Organometallics*, **19**, 1789 (2000).
- [55] B. Machura, I. Gryca. *Polyhedron*, **53**, 83 (2013).
- [56] T.I.A. Gerber, D.G. Luzipo, P. Mayer. *J. Coord. Chem.*, **59**, 1515 (2006).
- [57] J.B. Arterburn, I.M. Fogarty, K.A. Hall, K.C. Ott, J.C. Bryan. *Angew. Chem. Int. Ed.*, **35**, 2877 (1996).
- [58] (a) B. Machura, J. Miłek, R. Kruszynski, J. Kusz, J. Mroziński. *Polyhedron*, **27**, 1262 (2008); (b) B. Machura, R. Kruszynski, J. Kusz. *Polyhedron*, **27**, 1679 (2008); (c) B. Machura, M. Wolff, J. Kusz, R. Kruszynski. *Polyhedron*, **28**, 2949 (2009); (d) T.I.A. Gerber, D. Luzipo, P. Mayer. *J. Coord. Chem.*, **59**, 1521 (2006); (e) G. Bandoli, A. Dolmella, T.I.A. Gerber, D. Mpinda, J. Perils, J.G.H. Dupreez. *J. Coord. Chem.*, **55**, 823 (2002); (f) I.N. Booyens, M. Ismail, T.I.A. Gerber, M. Akerman, B. Van Brecht. *S. Afr. J. Chem.*, **65**, 174 (2012).
- [59] J.M. Botha, K. Umakoshi, Y. Sasaki. *Inorg. Chem.*, **37**, 1609 (1998).
- [60] I.N. Booyens, T.I.A. Gerber, P. Mayer. *Inorg. Chim. Acta*, **363**, 1292 (2010).
- [61] P. Traar, J.A. Schachner, L. Steiner, A. Sachse, M. Volpe, N.C. Mösch-Zanetti. *Inorg. Chem.*, **50**, 1983 (2011).
- [62] A. Barandov, U. Abram. *Polyhedron*, **28**, 1155 (2009).

- [63] M. Nishio. *CrystEngComm*, **6**, 130 (2004).
- [64] H.R. Khavasi, A.R. Salimi, H. Eshtiagh-Hosseini, M.M. Amini. *CrystEngComm*, **13**, 3710 (2011).
- [65] S. Majumder, A. Bhattacharya, J.P. Naskar, P. Mitra, S. Chowdhury. *Inorg. Chim. Acta*, **399**, 166 (2013).
- [66] I.N. Booyesen, M.B. Ismail, M.P. Akerman. *J. Coord. Chem.*, **66**, 4371 (2013).
- [67] B. Machura, M. Wolff, I. Gryca. *Inorg. Chim. Acta*, **370**, 7 (2011).
- [68] B. Machura, I. Gryca, M. Wolff. *Polyhedron*, **31**, 128 (2012).
- [69] D.H. Johnston, C.-C. Cheng, K.J. Campbell, H.H. Thorp. *Inorg. Chem.*, **33**, 6388 (1994).
- [70] V.W.W. Yam, Y.L. Pui, K.M.C. Wong, K.K. Cheung. *Inorg. Chim. Acta*, **300–302**, 721 (2000).
- [71] M.S. Ram, C.S. Johnson, R.L. Blackbourn, J.T. Hupp. *Inorg. Chem.*, **29**, 238 (1990).
- [72] S. Chowdhury, M. Nogami, A. Canlier, N. Koshino, Y. Ikeda. *Inorg. Chim. Acta*, **361**, 1524 (2008).
- [73] A. Bhattacharya, S. Majumder, J.P. Naskar, P. Mitra, S. Chowdhury. *J. Coord. Chem.*, **67**, 1413 (2014).
- [74] S. Trasatti. *Pure Appl. Chem.*, **58**, 955 (1986).
- [75] L.E. Fernandez, S. Horvath, S. Hammes-Schiffer. *J. Phys. Chem. C*, **116**, 3171 (2012).